Optimization of Costs and Self-Sufficiency for Roof Integrated Photovoltaic Technologies on Residential Buildings

DesignCon 2017

A Novel Generative Stochastic Model for High-Speed Interconnection Links

Simon De Ridder, Ghent University/imec
Simon.DeRidder@UGent.be

Paolo Manfredi, Ghent University/imec

Jan De Geest, Amphenol-FCI

Tom Dhaene, Ghent University/imec

Daniël De Zutter, Ghent University/imec

Dries Vande Ginste, Ghent University/imec

Abstract

In this paper we introduce a new modeling approach to create a generative model for stochastic link responses. The proposed scheme starts from a limited set of simulated or measured ‘training samples’, which are first represented by a rational model using vector fitting with common poles. Next, the generative model is built, leveraging the residues' stochastic distribution, via a principal component analysis and kernel density estimation. Then, in a post-processing phase, non-passive samples are discarded. The novel method is applied to a commercial connector footprint, a multi-conductor transmission line, and a complete link composed of the cascade connection of the former components.

Author(s) biography

Simon De Ridder was born in 1992. He received the M.Sc. degree in physics and astronomy from Ghent University, in 2015. He is currently a Ph.D. student in electrical engineering at Ghent University. His work focuses on stochastic modeling of electrical systems and machine learning applications.

Paolo Manfredi was born in 1985. He received the M.Sc. degree in electronic engineering from the Politecnico di Torino, Turin, Italy, in 2009, and the Ph.D. degree in information and communication technology from the Scuola Interpolitecnica di Dottorato, Politecnico di Torino, in 2013. He is currently a Postdoctoral Research Fellow with the Research Fund- Flanders (FWO), Electromagnetics Group, Department of Information Technology, Ghent University, Ghent, Belgium.

Jan De Geest is a Senior Staff R&D Signal Integrity Engineer at Amphenol-FCI. He received the degree in electrical engineering from the University of Ghent, Belgium in 1994 and the degree in supplementary studies in aerospace techniques from the University of Brussels, Belgium in 1995. From September 1995 to December 1999 he worked as a research assistant at the Department of Information Technology (INTEC) of the University of Ghent, where he received the PhD degree in electrical engineering in 2000. Since January 2000 he has been working for AFCI. His work focuses on the design, modeling, characterization and optimization of high-speed connectors and interconnection links.

Tom Dhaene received the Ph.D. degree in electrotechnical engineering from Ghent University, Ghent, Belgium, in 1993. From 1989 to 1993, he was a Research Assistant with the Department of Information Technology, Ghent University. In 1993, he was with the EDA company Alphabit (now part of Keysight Technologies). He was one of the key developers of the planar EM simulator ADS Momentum. Since 2007, he has been a Full Professor with the Department of Information Technology (INTEC), Ghent University & iMinds. He has authored/coauthored more than 300 peer-reviewed papers and abstracts in international conference proceedings, journals, and books. He is the holder of five U.S. patents. His research interests include different aspects of full-wave electromagnetic circuit modeling, transient simulation, and time-domain characterization of high-frequency and high-speed interconnections.

Daniël De Zutter (M. Sc. 1976, Ph. D. 1981, Habilitation 1984, Fellow IEEE 2000) is a full professor of Electromagnetics at Ghent University. He contributed to more than 240 international journal papers. Between 2004 and 2008 he served as the Dean of the Faculty of Engineering and is now the head of the Department of Information Technology.

Dries Vande Ginste received the M.S. degree and the Ph.D. degree in electrical engineering from Ghent University, Gent, Belgium, in 2000 and 2005, respectively. He is an Associate Professor with the Department of Information Technology, Ghent University and a Guest Professor at IMEC. His research interests include computational electromagnetics, electromagnetic compatibility, signal and power integrity, and antenna design.

1. Introduction

The impact of variability in electronic devices has sparked a growing interest. This variability is induced by manufacturing tolerances and, also owing to miniaturization and bandwidth requirements, nowadays it has a considerable effect on the signal integrity performance and on the overall functioning of the device. Many techniques, such as generalized Polynomial Chaos (gPC) [1] [2] [3], have been successfully used to model this variability.
These models do require, however, a precise knowledge of the stochastic distribution of the physical parameters that are subject to variability. When many such parameters come into play, a large set of input data (or responses) is needed and, consequently, the simulation time or the manufacturing and measurement process inhibits the construction of accurate gPC models.

The novel modeling approach presented in this paper, by contrast, assumes only a limited set of responses as a 'training set' and builds a generative model from them.
Thereto, the training samples are first represented by a rational model through the well-established Vector Fitting (VF) [4] [5] [6] technique. The rational model consists of a finite set of residues and poles. To maintain stability, all samples are fitted simultaneously to obtain a set of common poles. Secondly, the dimensionality of the residues is reduced by means of a Principal Component Analysis (PCA) [7] [8] [9]. Third, in the lower-dimensional projected space, the stochastic distribution of the residues is modeled by a multivariate Kernel Density Estimation (KDE) [10] [11] [12], allowing the generation of new samples from the modeled distribution. Finally, in a post-processing phase, the non-passive samples are discarded in order to retain only physically consistent responses.

The proposed modeling strategy is validated by application to the following three examples. First, a commercial connector footprint with 40 randomly varying parameters is modeled, starting from its simulated scattering (S-)parameter responses. In this case, the connector footprint's uncertainty stems from the manufacturing tolerances, which lead to variability of its geometrical dimensions. Second, a multi-conductor transmission line is modeled. Here, the variability is induced by the randomness of the relative permittivity of the board material (typically FR-4), which is captured via the per-unit-of-length transmission line (RLGC) parameters of the interconnect structure under investigation. Third, the generated samples of the previous two examples are combined to form a stochastic representation for the complete link, i.e. the concatenation of a footprint, a transmission line and another footprint. The properties of the generated samples are found to closely match those of the original data distribution, as verified by comparison with a significant amount of additionally simulated validation samples.

The comprehensive theoretical description of the modeling formalism, together with the illustrative validation and application examples, make it apparent that the proposed strategy is immediately applicable to state-of-the-art interconnect design. To reach the usually very stringent constraints, the designer can now readily simulate the influence of manufacturing on his/her nominal design (of individual building blocks or of a complete link), and make the necessary adjustments to meet the overall link specifications.

2. Proposed stochastic modeling strategy

Consider an n-port passive network, e.g. a multi-conductor transmission line (MTL) or a connector, subject to variability of its dimensions or materials. In what follows, we assume that a small training set of K S-parameter samples is readily obtained for this device, through either measurement or simulation.

Figure 1 shows a flowchart of the proposed method. Starting from the training samples, the three main steps (VF, PCA and KDE) lead to the construction of the generative stochastic model. From this generative model, new samples are obtained via inverse PCA and VF reconstruction and subsequently subjected to a passivity test, rejecting non-passive samples. Each step is discussed in the following subsections.

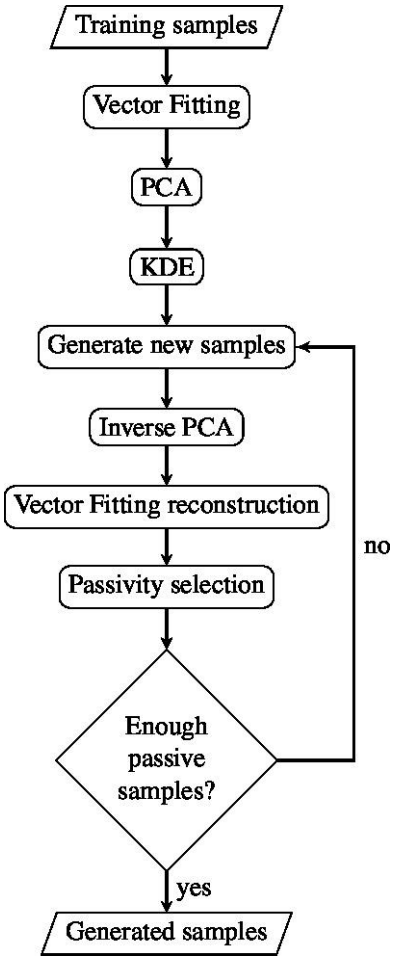

Figure 1: Flowchart of the proposed method.

2.1 Vector Fitting (VF)

In the first modeling step, the training set of measured or simulated S-parameter samples is approximated by a sum of partial fractions using the Vector Fitting algorithm [4] [5] [6]:

$$S(s) \approx \sum_{i=1}^{N} \frac{R_i}{s - a_i} + Ds + E,$$

Equation 1: Vector Fitting approximation.

with s the complex frequency, $\{a_i\}$ the N (real or complex) poles, $\{R_i\}$ the corresponding N (real or complex) residue matrices, and D and E optional real matrices that provide a linear and constant component respectively, as such describing the potential asymptotic behavior. The VF algorithm enforces stability by locating all poles in the left half of the complex plane and by requiring the poles either to be real or to appear as a pair of complex conjugate poles in two expansion terms.

To avoid unstable generated samples later on, the training samples are first fitted all at once to obtain a set of common poles. Then, each training sample is fitted again with these common poles to obtain its individual residue matrix. These residue matrices now form a frequency-independent representation of each sample. As they are (non-linearly) correlated, all elements of each residue matrix must be modeled simultaneously.

2.2 Principal Component Analysis (PCA)

As each of the N residues is a $n \times n$ matrix, this yields Nn^2 correlated (complex) variables to model, or when the device under study is reciprocal, $Nn(n+1)/2$ variables. For a large number of ports (n large) and/or when considering a large frequency range (many expansion terms needed, thus large N), this leads to a considerable amount of variables. Therefore, during the second step of the model construction, a Principal Component Analysis [7] [8] [9] is applied to these variables to reduce the dimensionality for further modeling. This technique produces new variables from the eigenvectors of the covariance matrix of the old, original variables with the highest eigenvalues. Another advantage of applying PCA is that it removes linear correlation between variables, such that only nonlinear correlations remain present.

2.3 Kernel Density Estimation (KDE)

The third and final modeling step deals with the estimation of the distribution of the residue elements in the reduced space. This is performed by means of Kernel Density Estimation. This technique approximates a probability distribution function (PDF) as the sum of kernels centered on each training point. These kernels can be any central PDF. The most widely used, in part because of computational tractability, is the multivariate Gaussian kernel. In what follows, such Gaussian kernels were applied.

2.4 Generating new samples

After the aforementioned three-step model building phase is completed, it is possible to generate new samples as follows. First, the final KDE model is used to generate new

points in the reduced space. Thereto, it suffices to pick a training point at random and sample from its kernel. Secondly, the samples are projected back onto the space of residue matrix elements (inverse PCA step), from which new residue matrix samples are constructed. Finally, the generated residue matrices are combined using Equation 1 to yield S-parameter samples.

2.5 Passivity selection

In a post-processing step, the passivity of each generated sample is verified. Any non-passive sample is discarded and new samples are generated until enough passive samples are obtained (see Figure 1). Alternatively, a passivity *enforcement* scheme could be applied, but this may introduce a bias toward nearly non-passive samples.

3. Applications

To demonstrate its validity, the proposed method is applied to a commercial connector footprint, a multi-conductor transmission line, and finally, to a concatenation of the former two elements.

3.1 Commercial connector footprint

In this section the method is applied to a commercial 16-port connector footprint. The model was trained using 50 simulated samples, and 15 terms were used in the VF expansion ($N = 15$ in Equation 1). Figure 2 shows the port numbering used in this and following examples.

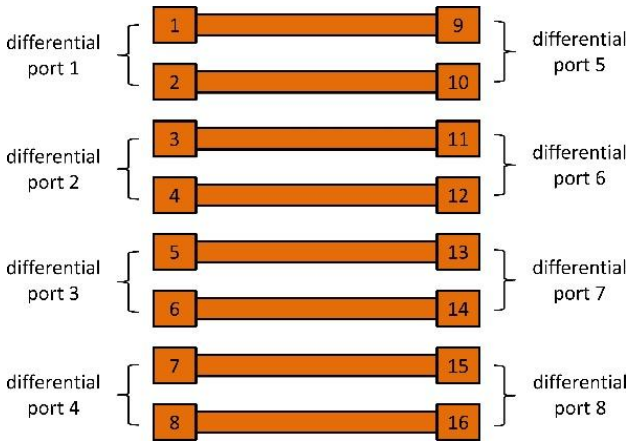

Figure 2: The footprint's differential port

The accuracy of the distribution of the newly generated samples is assessed from Figure 3-Figure 10. In these figures, 950 simulated validation samples are shown in the background (green lines) with 1000 generated samples superposed on top of them (blue lines). The 50 training samples are shown in the foreground (red lines). The black lines indicate the minimum and maximum response, as obtained from the validation samples. Note that the modal S-parameters are shown (not the single-ended ones), as the footprint is intended for usage in a differential signaling scheme. From these figures it is concluded that, apart from small and unavoidable discrepancies caused by the finite number of validation samples and the VF approximation, the agreement between the distributions of the simulated and generated samples is very good.

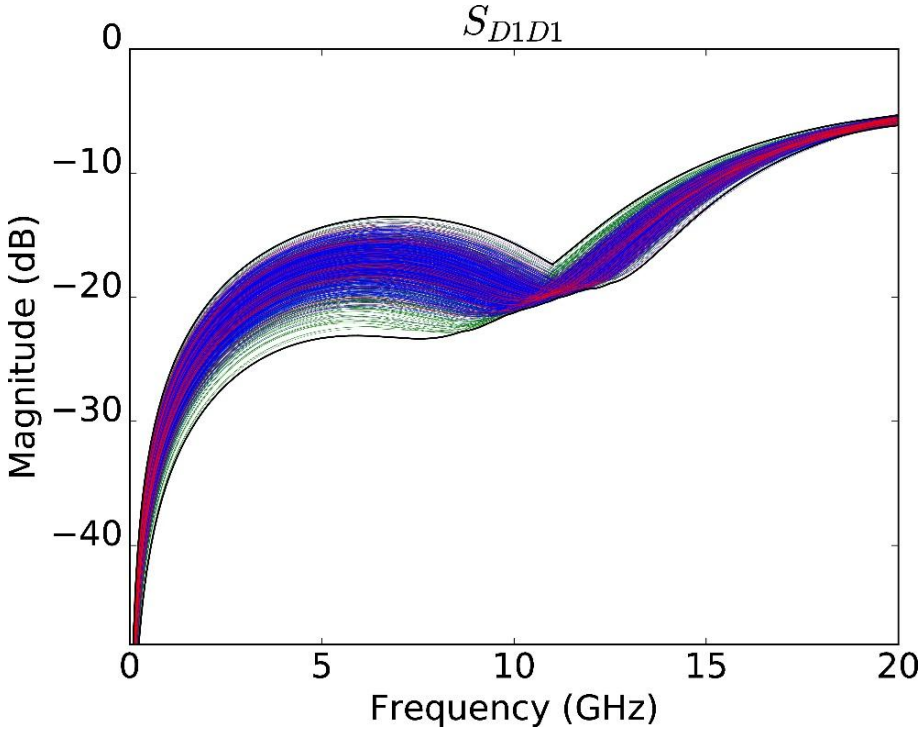

Figure 3: Magnitude of the footprint's differential mode S-parameter S_{D1D1}. Validation samples are shown in green, generated samples in blue, and training samples in red. The two black lines indicate the minimum and the maximum of the validation samples.

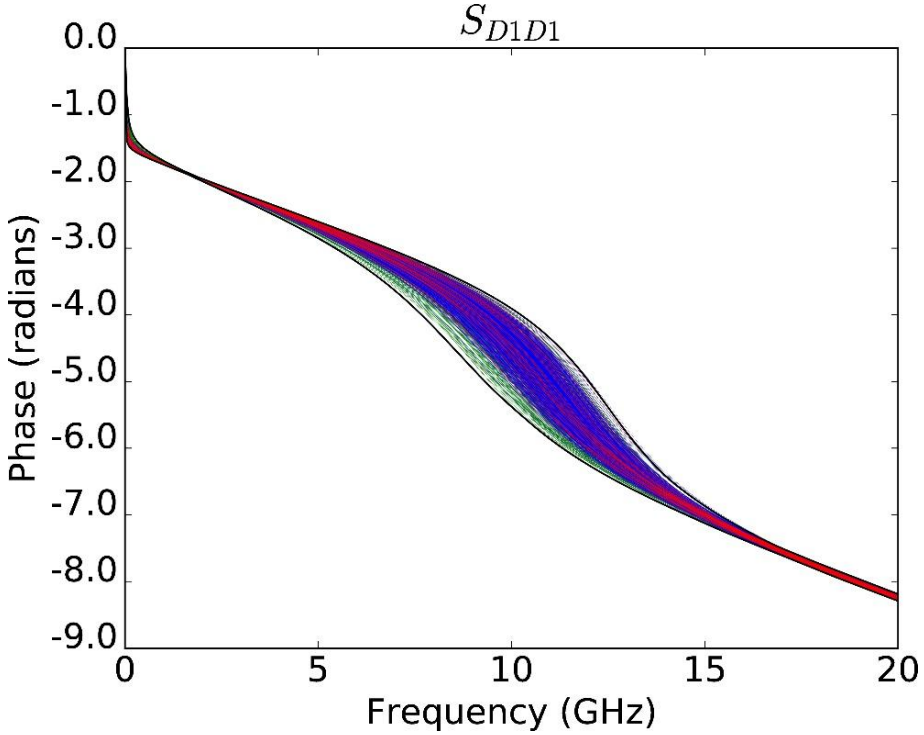

Figure 4: Unwrapped phase of the footprint's differential mode S-parameter S_{D1D1}. The colors are as in the previous figure.

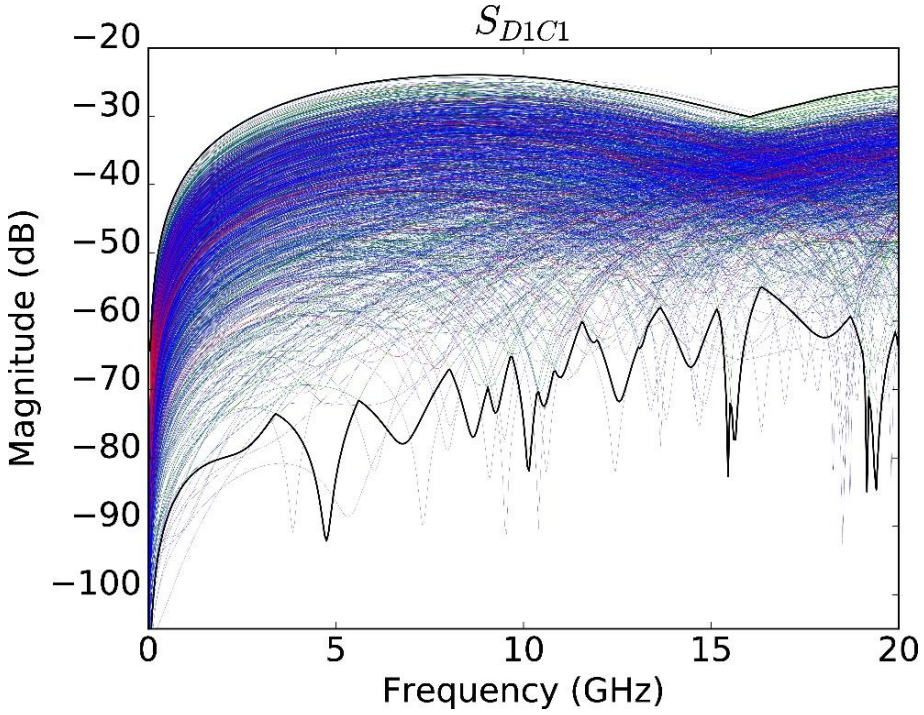

Figure 5: Magnitude of the footprint's mode conversion S-parameter S_{D1C1}. The colors are as in the previous figures.

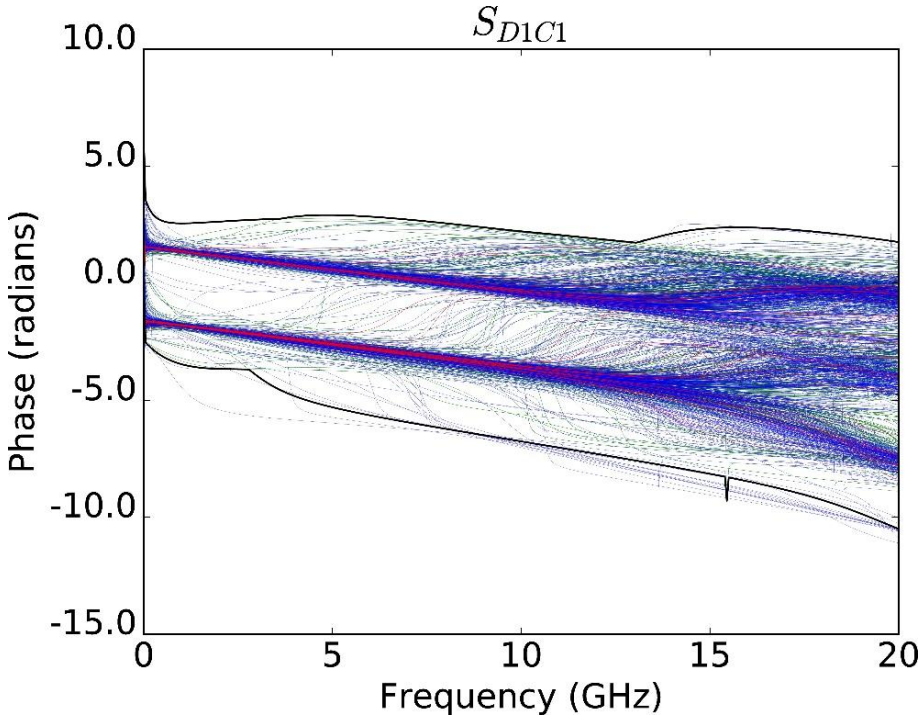

Figure 6: Unwrapped phase of footprint's mode conversion S-parameter S_{D1C1}. The colors are as in the previous figures.

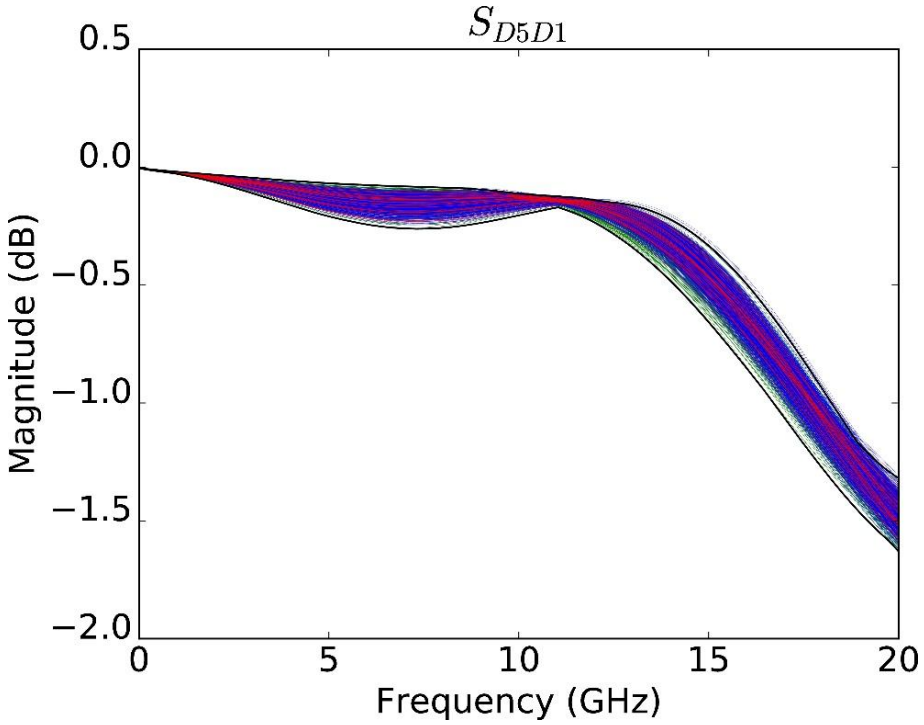

Figure 7: Magnitude of the footprint's differential transmission S-parameter S_{D5D1}. The colors are as in the previous figures.

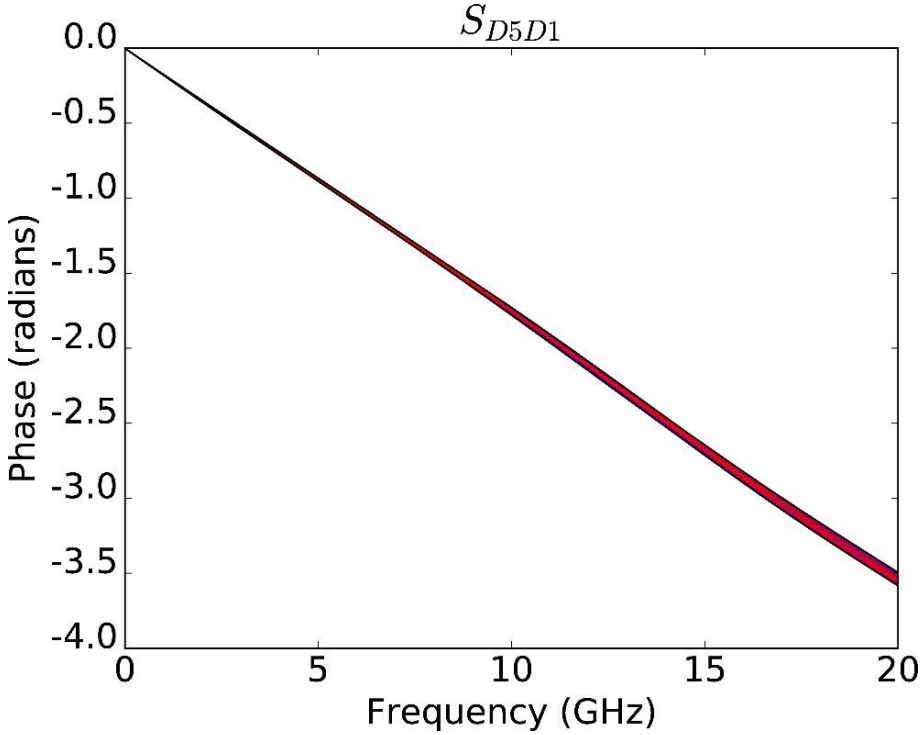

Figure 8: Unwrapped phase of the footprint's differential transmission S-parameter S_{D5D1}. The colors are as in the previous figures.

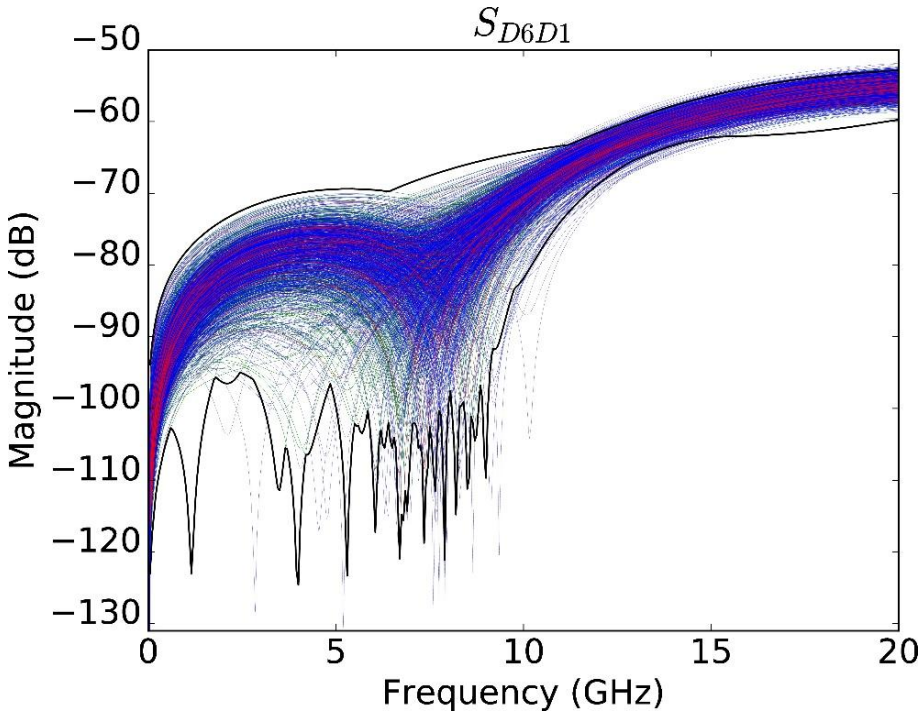

Figure 9: Magnitude of the footprint's differential far-end crosstalk S-parameter S_{D6D1}. The colors are as in the previous figures.

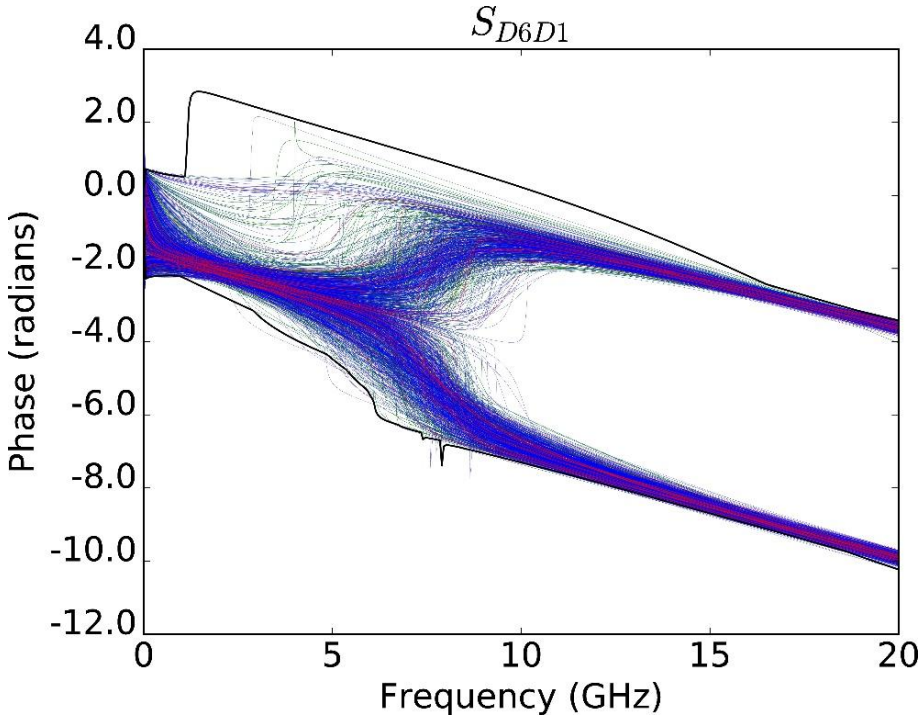

Figure 10: Unwrapped phase of the footprint's differential far-end crosstalk S-parameter S_{D6D1}. The colors are as in the previous figures.

3.2 Multi-conductor stripline

As a second example, we study a 5 cm long multi-conductor transmission line in stripline topology, with variability stemming from the relative permittivity of its substrate. For later concatenation with the connector footprint, 8 coupled striplines, and 50 training samples were used. Figure 11 shows the dimensions of the stripline. The port numbering is the same as for the footprint (see Figure 2).

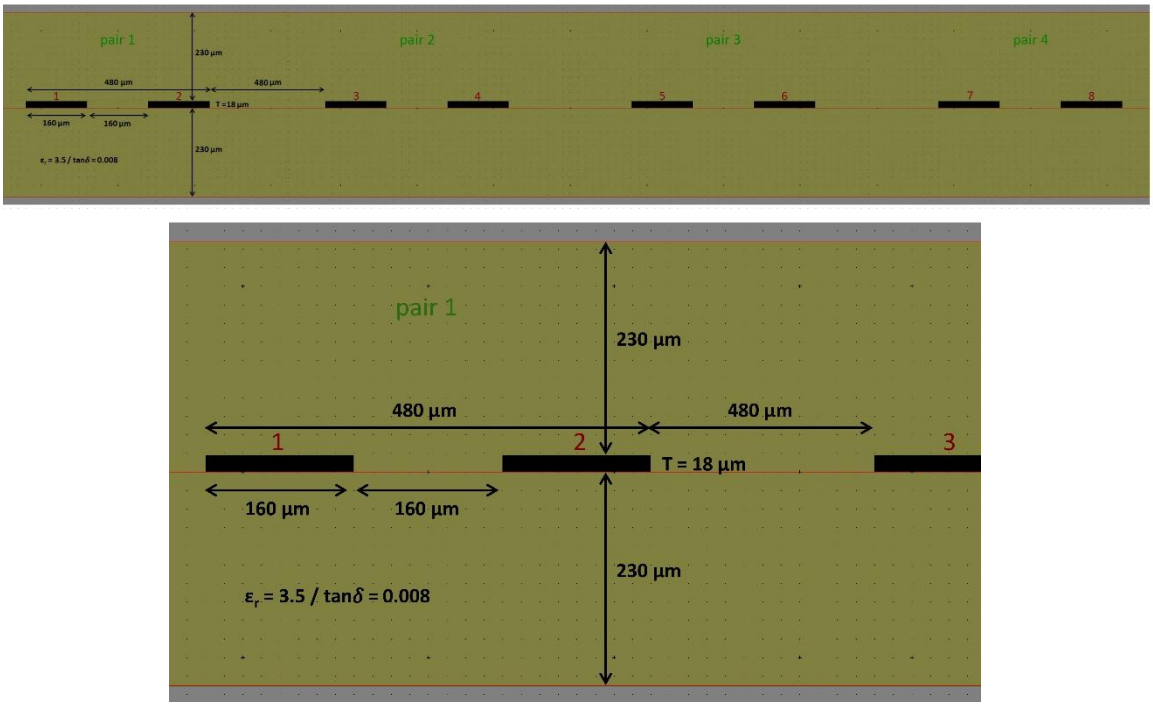

Figure 11: Nominal dimensions of the MTL stripline. The distance between line pairs is not shown at scale.

As modeling the S-parameters of a long transmission line over a broad frequency range (here: from 0 to 20 GHz) would require a very large amount of terms in Equation 1 (this is a longstanding issue with VF), we rather model its per-unit-of-length (p.u.l.) RLGC-parameters. This simply requires a relaxation of the stability requirement in the model, taking the correlations between these p.u.l. parameter matrices into account, and a conversion to S-parameters before the passivity check. This way, only 30 VF terms were needed.

Similarly to the footprint model, the accuracy of the generated distribution is observed in Figure 12 and Figure 13, where the self-conductance (G_{11}) and self-capacitance (C_{11}) of the first signal conductor in the TML have been plotted (all resistance and inductance parameters are constant, as only the relative permittivity varies between samples), and in Figure 14-Figure 21, where some of the modal S-parameters are shown. In these figures, the validation samples were converted from p.u.l. parameters to S-parameters in the same way as the generated samples. Again, these figures show a very good agreement between validation and generated distributions.

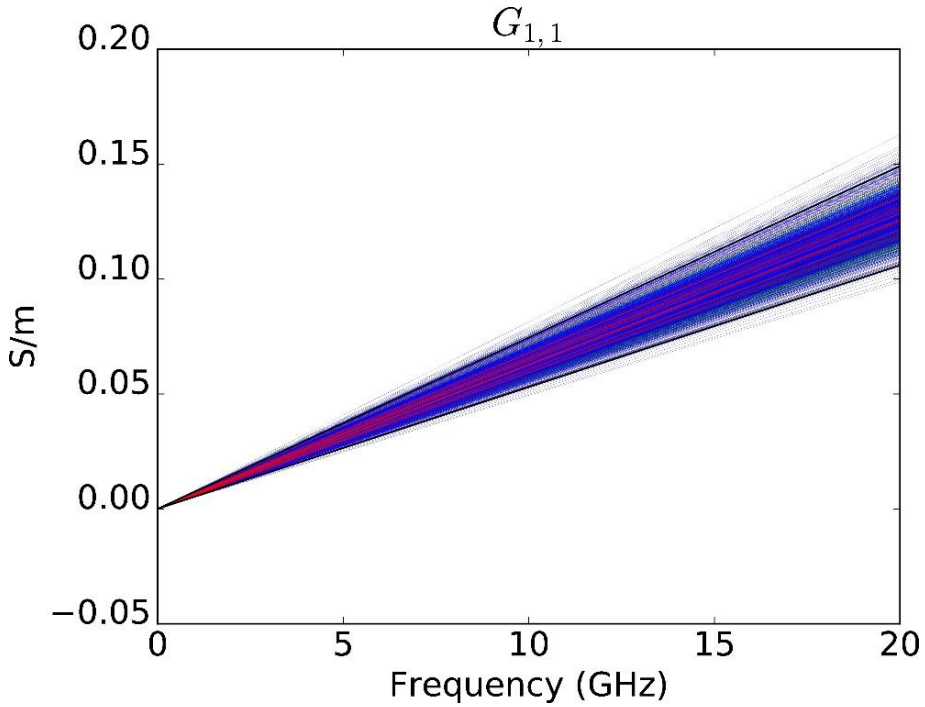

Figure 12: p.u.l. parameter G_{11} of the stripline. The colors are as in the previous figures.

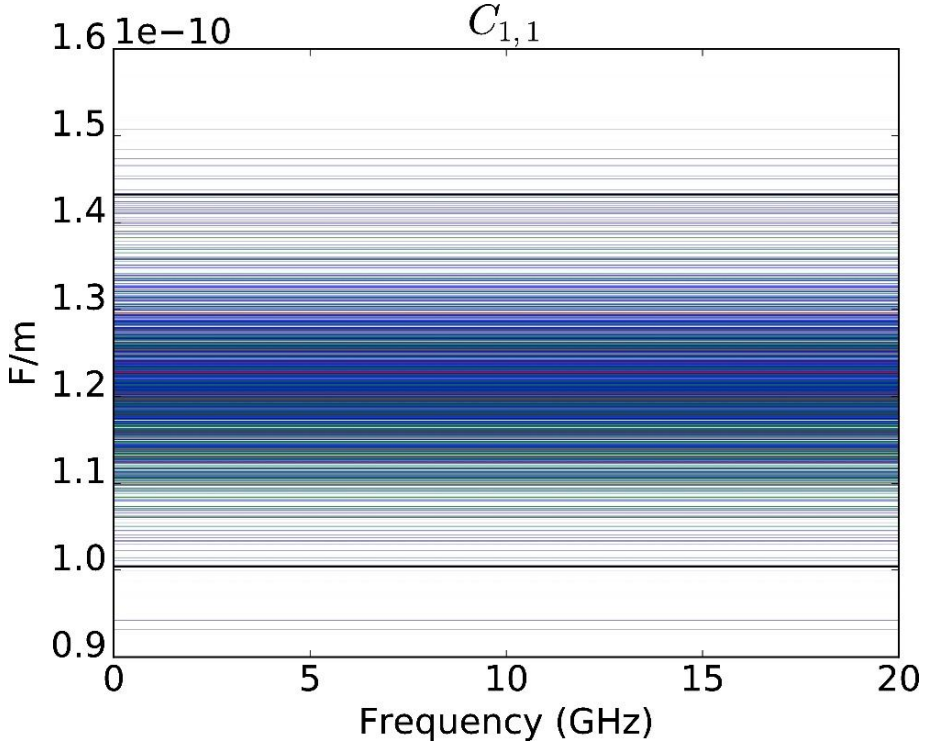

Figure 13: p.u.l. parameter C_{11} of the stripline. The colors are as in the previous figures.

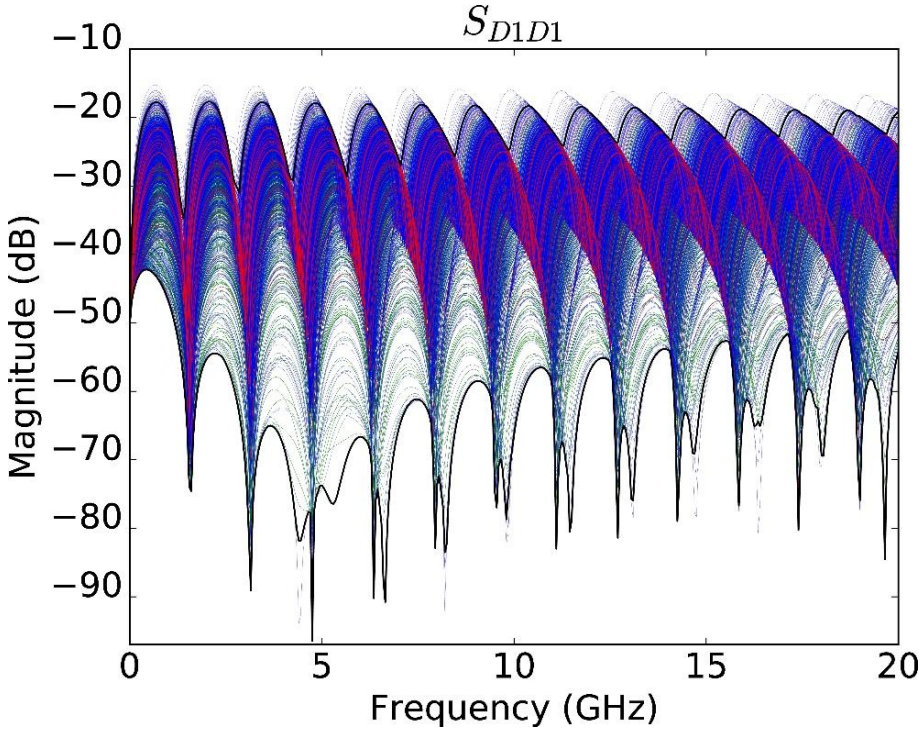

Figure 14: Magnitude of the MTL's differential mode S-parameter S_{D1D1}. The colors are as in the previous figures.

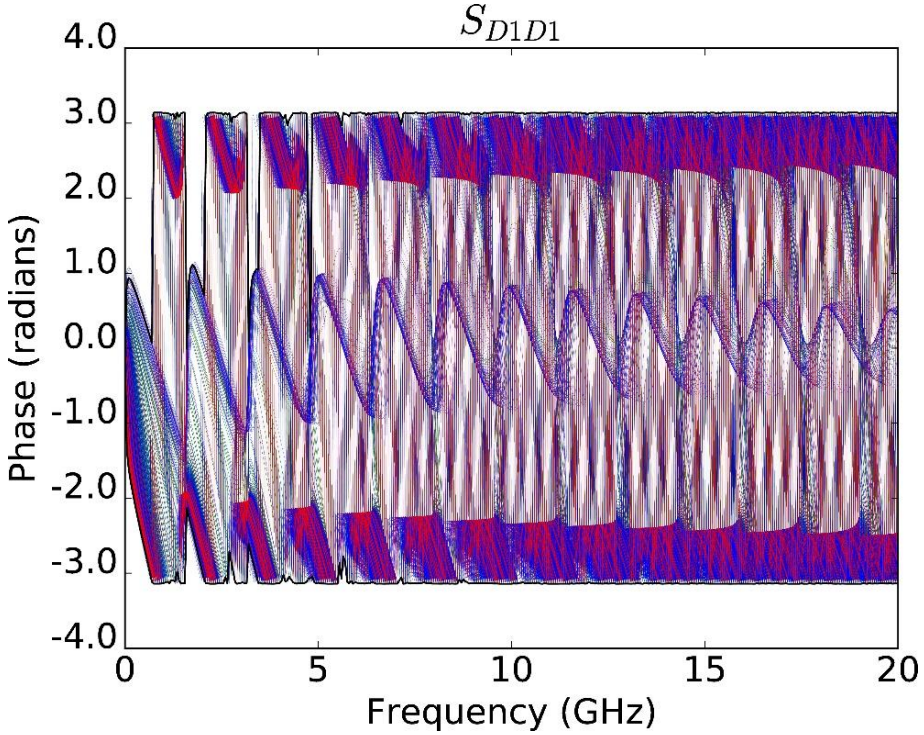

Figure 15: Wrapped phase of the MTL's differential mode S-parameter S_{D1D1}. The colors are as in the previous figures.

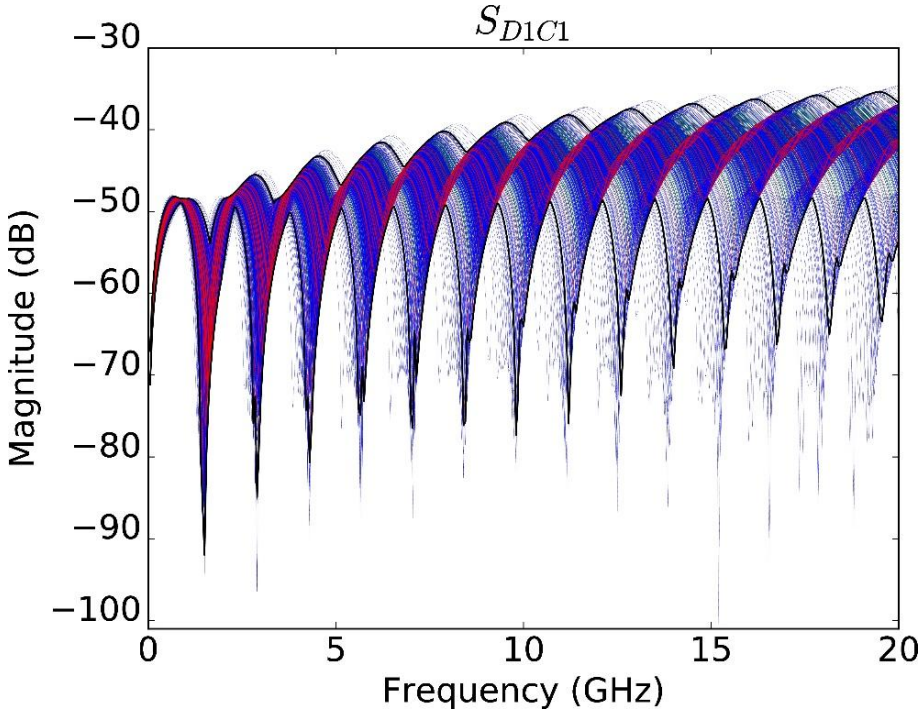

Figure 16: Magnitude of the MTL's mode conversion S-parameter S_{D1C1}. The colors are as in the previous figures.

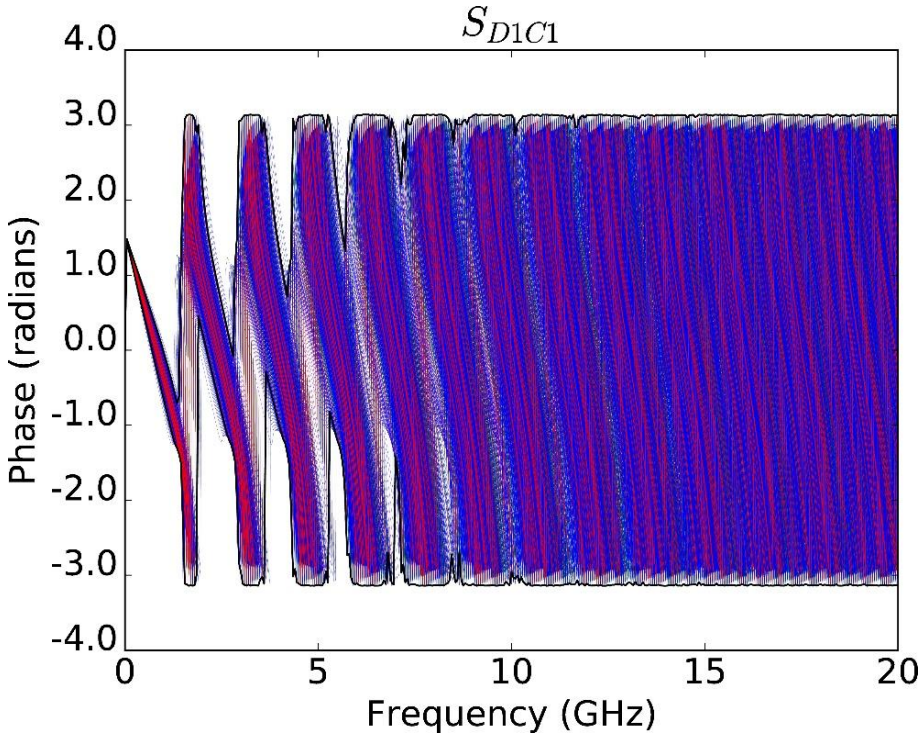

Figure 17: Wrapped phase of the MTL's mode conversion S-parameter S_{D1C1}. The colors are as in the previous figures.

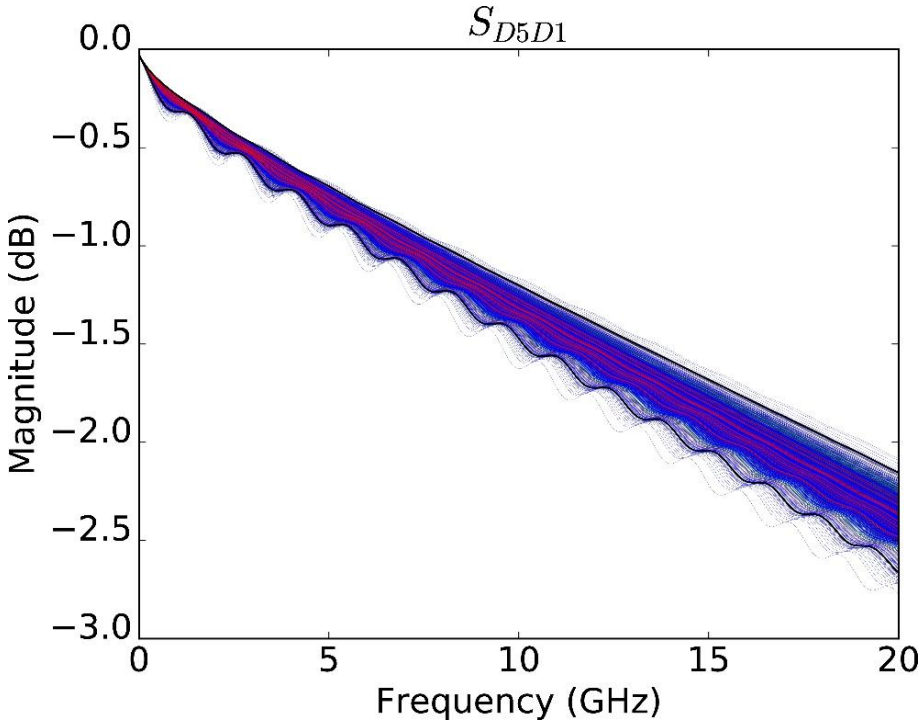

Figure 18: Magnitude of the MTL's differential transmission S-parameter S_{D5D1}. The colors are as in the previous figures.

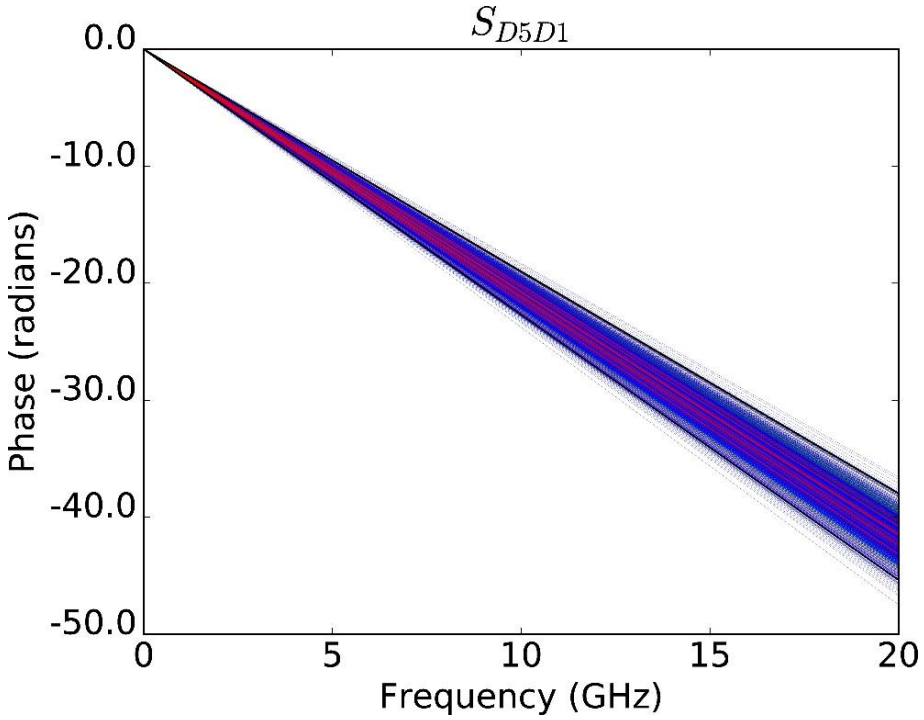

Figure 19: Unwrapped phase of the MTL's differential transmission S-parameter S_{D5D1}. The colors are as in the previous figures.

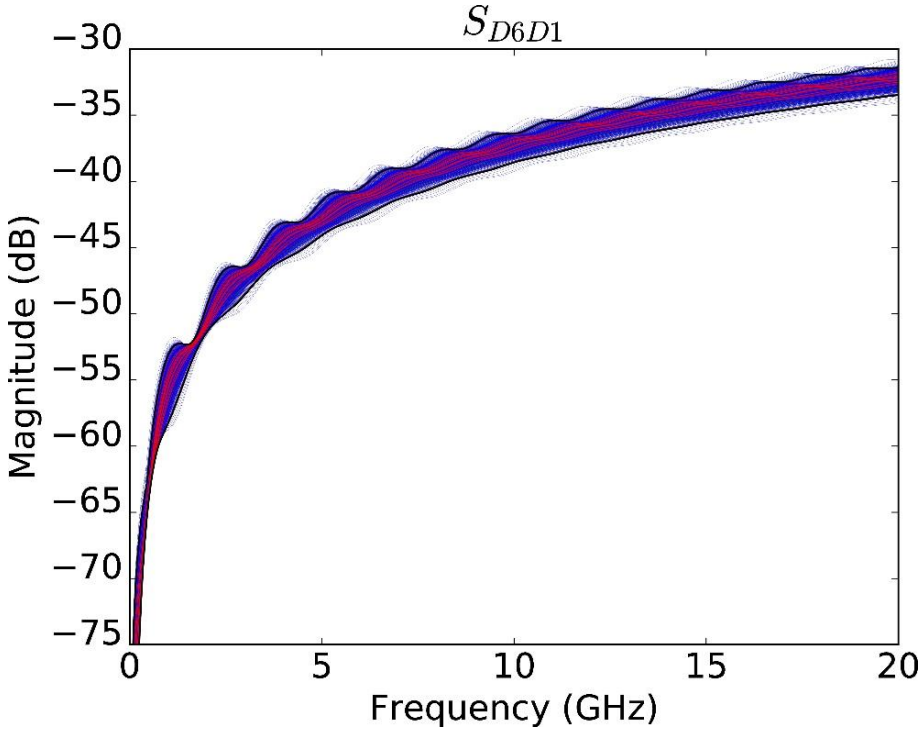

Figure 20: Magnitude of the MTL's differential far-end crosstalk S-parameter S_{D6D1}. The colors are as in the previous figures.

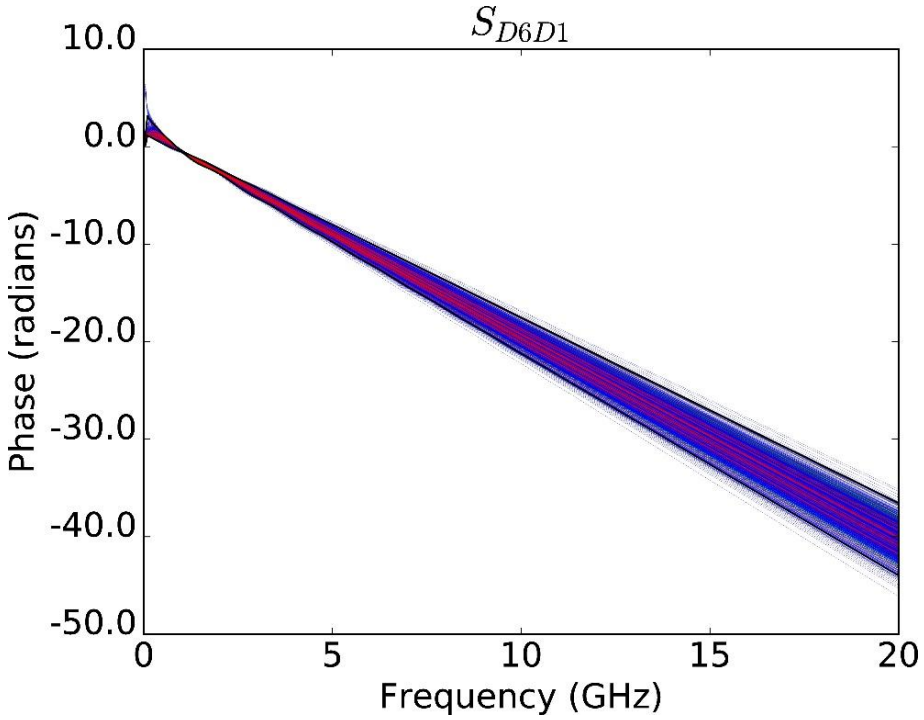

Figure 21: Unwrapped phase of the MTL's differential far-end crosstalk S-parameter S_{D6D1}. The colors are as in the previous figures.

3.3 Complete interconnection link

In this section we further explore the applicability of the new modeling technique by considering a cascade of the previously studied components, being the connector footprint and the MTL. We now use the samples generated for both the footprint and the stripline and concatenate randomly selected triplets of footprint, MTL stripline and footprint. The same is done for the validation and training samples and the distributions of the entire link are compared. Figure 22 shows a schematic of this concatenation.

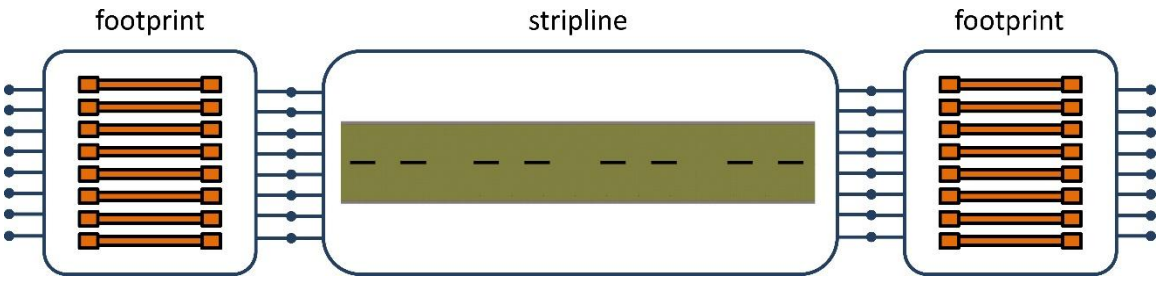

Figure 22: Schematic representation of the complete interconnect link.

The results are shown in Figure 23-Figure 30. As for the previous applications, only minor discrepancies between the distributions of the generated and validation samples are observed, while overall there is a very good agreement, despite the rather complex behavior of the S-parameters over the covered frequency range.

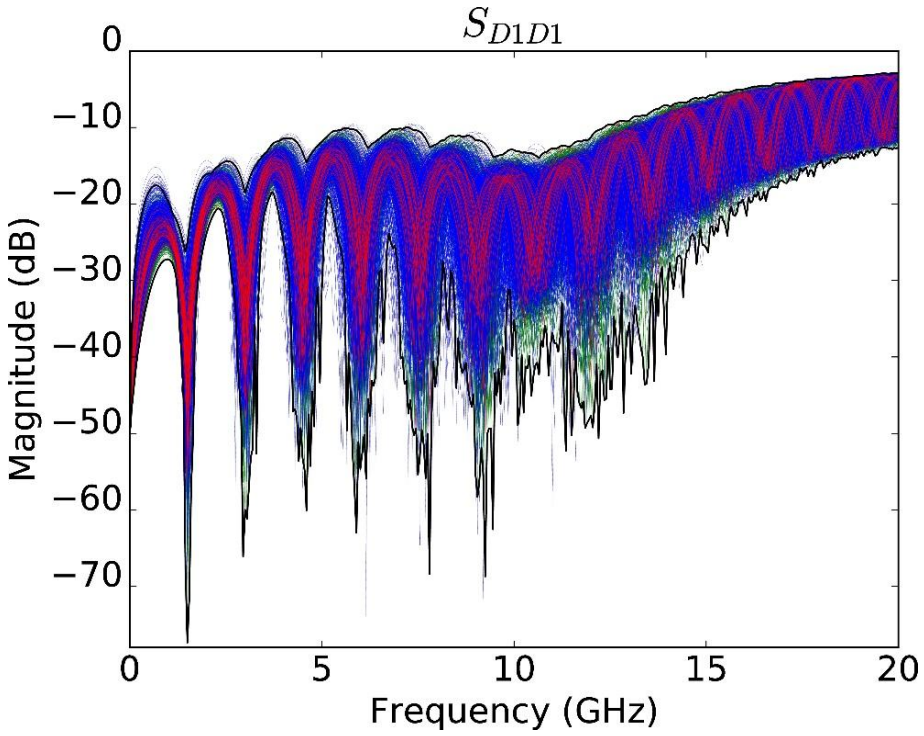

Figure 23: Magnitude of the complete link's differential mode S-parameter S_{D1D1}. The colors are as in the previous figures.

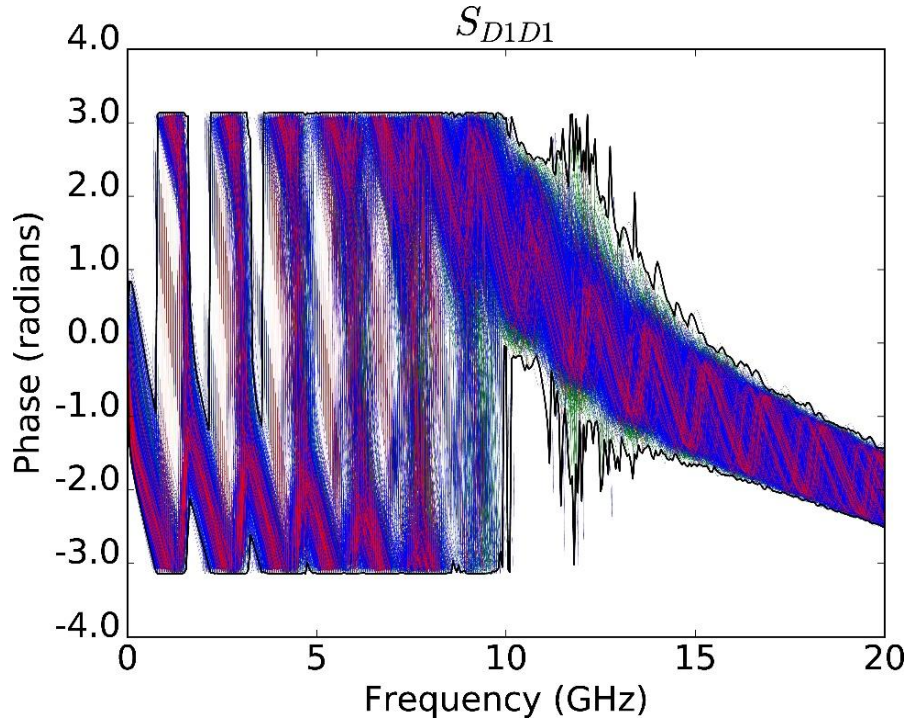

Figure 24: Wrapped phase of the complete link's differential mode S-parameter S_{D1D1}. The colors are as in the previous figures.

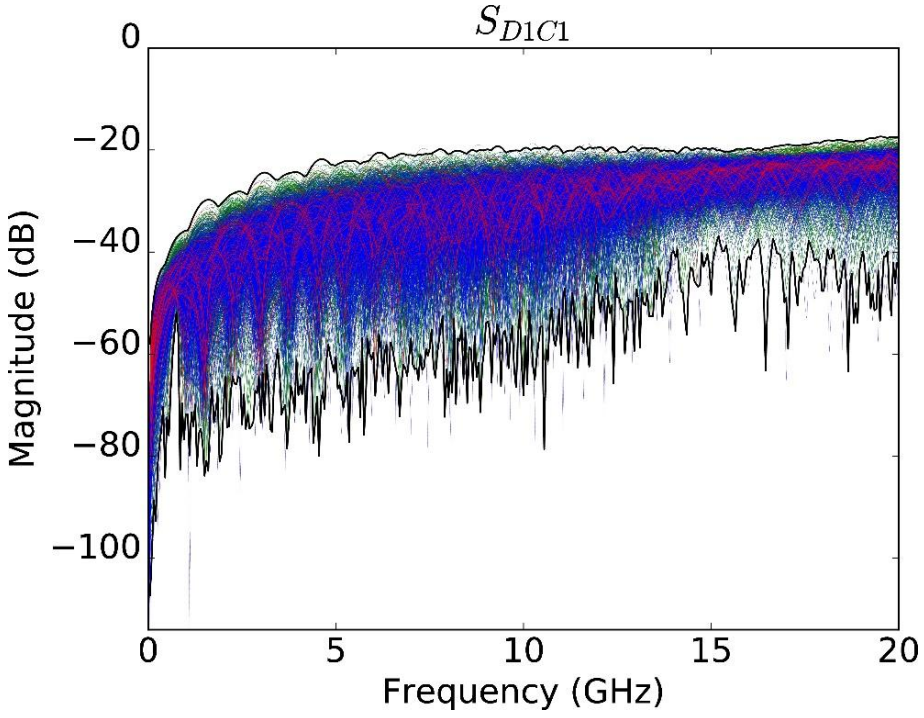

Figure 25: Magnitude of the complete link's mode conversion S-parameter S_{D1C1}. The colors are as in the previous figures.

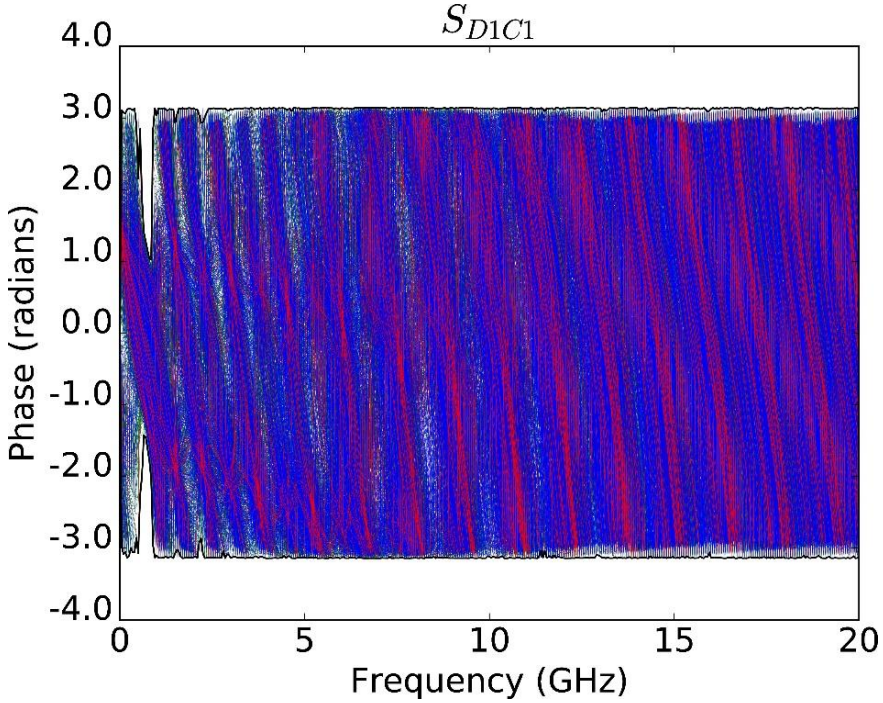

Figure 26: Wrapped phase of the complete link's mode conversion S-parameter S_{D1C1}. The colors are as in the previous figures.

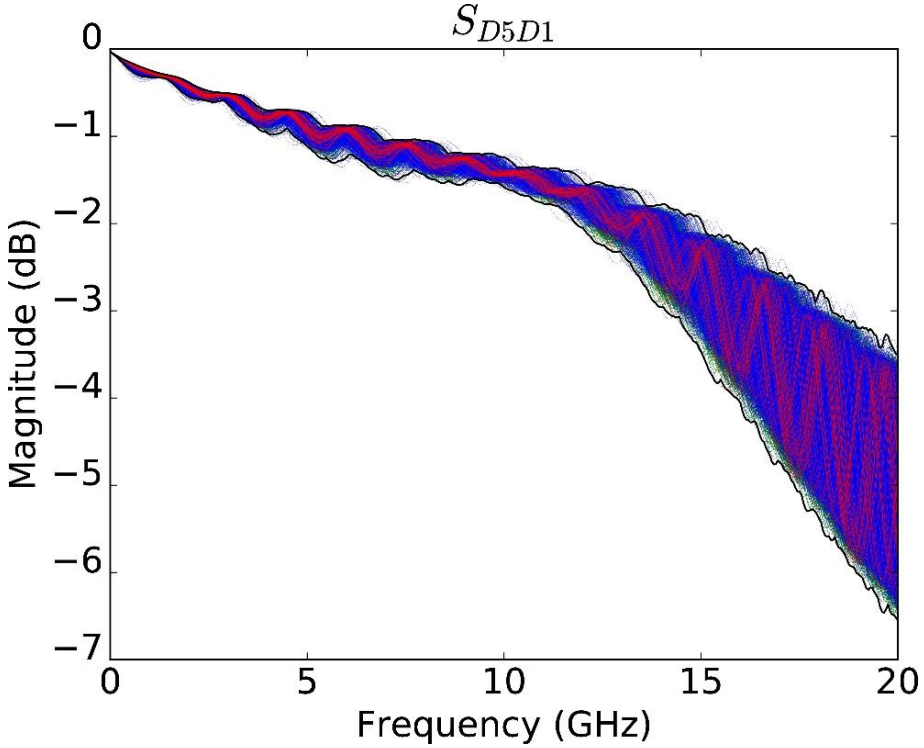

Figure 27: Magnitude of the complete link's differential transmission S-parameter S_{D5D1}. The colors are as in the previous figures.

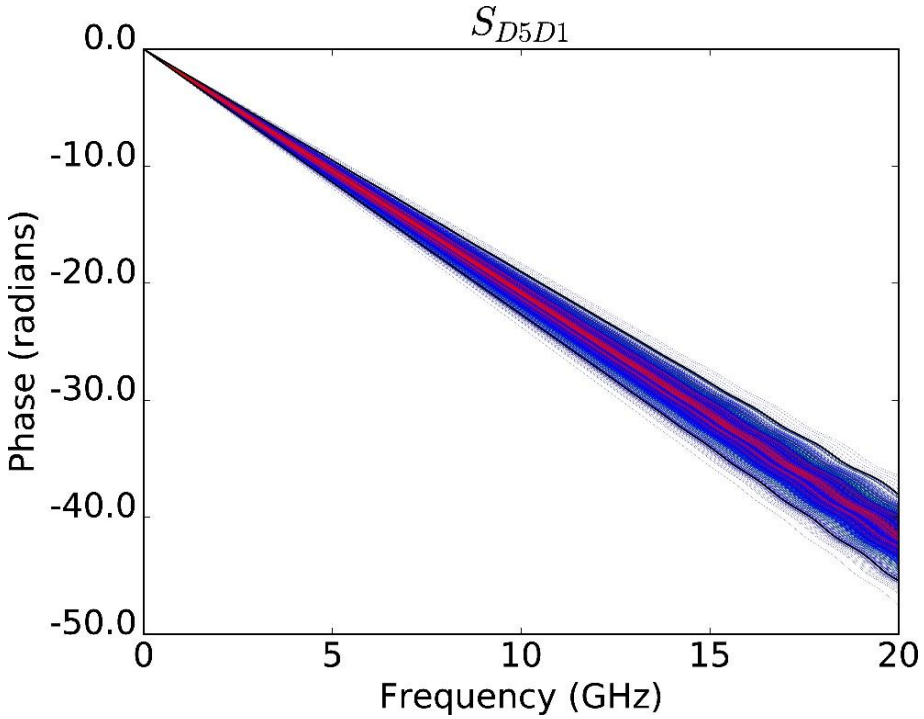

Figure 28: Unwrapped phase of the complete link's differential transmission S-parameter S_{D5D1}. The colors are as in the previous figures.

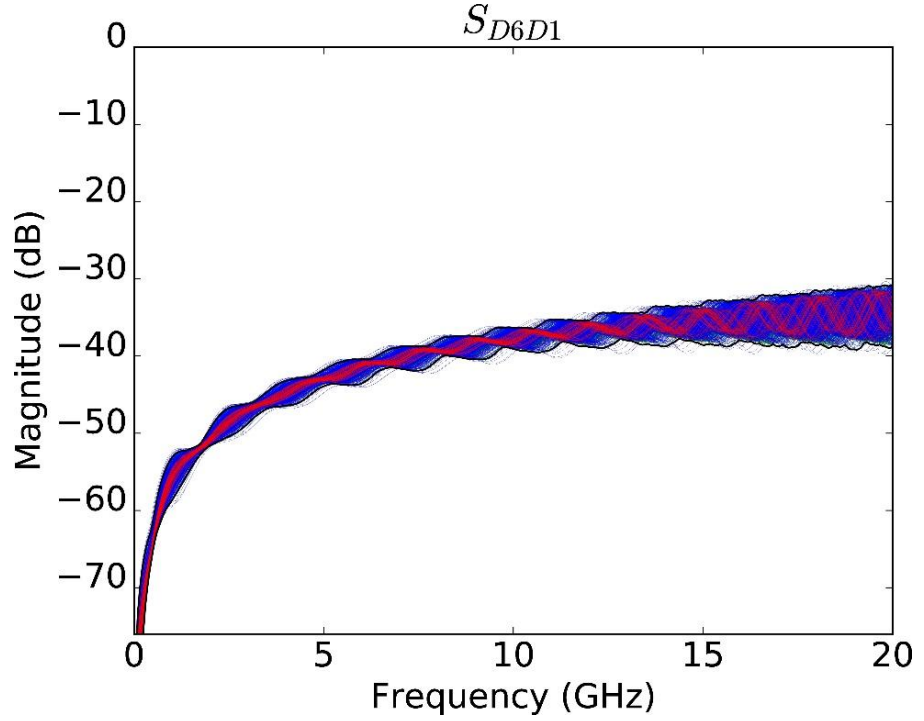

Figure 29: Magnitude of the complete link's differential far-end crosstalk S-parameter S_{D6D1}. The colors are as in the previous figures.

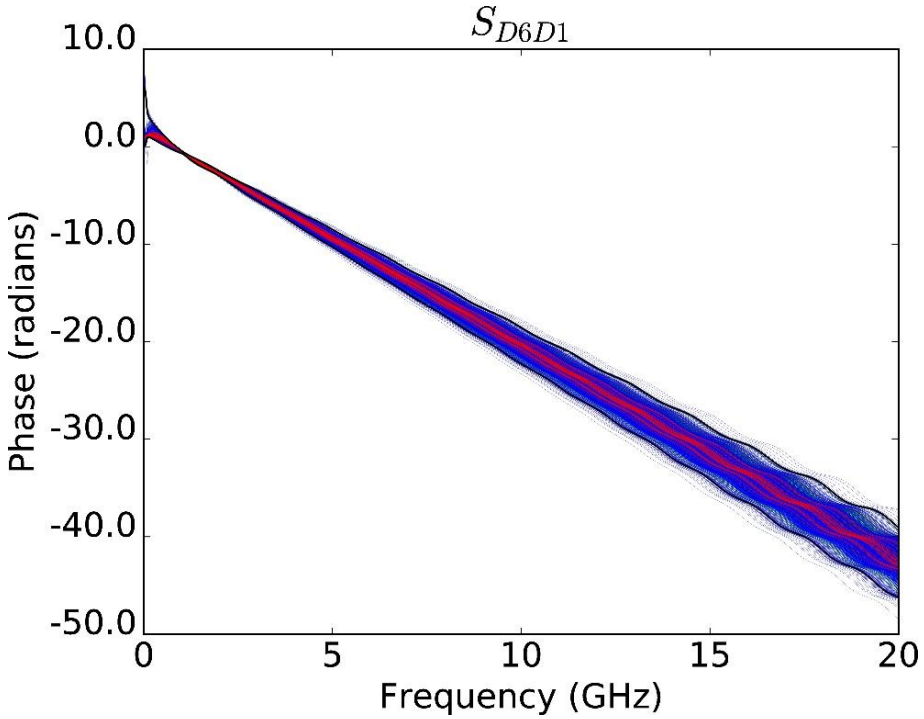

Figure 30: Unwrapped phase of the complete link's differential far-end crosstalk S-parameter S_{D6D1}. The colors are as in the previous figures.

4. Conclusion

In this paper, a novel method is proposed to generate representative S-parameter samples of interconnection links that are prone to manufacturing variability. Starting from a small training set of S-parameter data, first a rational model is fitted to these training samples' S-parameters and then the residues are modeled by means of PCA and KDE. A post-processing passivity selection step ensures physical consistency of the generated samples. In this manner, many samples are efficiently generated and their distribution closely matches that of the original data.

The applicability is verified by modeling a connector footprint, a multi-conductor transmission line and a complete link composed of the two former elements. The proposed method yields a considerable gain in efficiency when a large number of samples is needed, and when measurement or simulation proves to be too time- or cost-expensive.

References

[1] P. Manfredi, D. Vande Ginste, D. De Zutter and F. G. Cavavero, "Uncertainty Assessment of Lossy and Dispersive Lines in SPICE-Type Environments," *IEEE Transactions on Components, Packaging and Manufacturing Technology*, vol. 3, no. 7, pp. 1252-1258, July 2013.

[2] A. Rong and A. C. Cangellaris, "Interconnect transient simulation in the presence of layout and routing uncertainty," in *IEEE 20th Conf. Elect. Performance Electron.*

Packaging Syst., San Jose, CA, 2011.

[3] M. R. Rufuie, E. Gad, M. Nahkla and R. Achar, "Generalized Hermite Polynomial Chaos for Variability Analysis of Macromodels Embedded in Nonlinear Circuits," *IEEE Transactions on Components, Packaging and Manufacturing Technology,* vol. 4, no. 4, pp. 673-684, April 2014.

[4] B. Gustavsen and A. Semlyen, "Rational approximation of frequency domain responses by vector fitting," *IEEE Transactions on Power Delivery,* vol. 14, no. 3, pp. 1052-1061, July 1999.

[5] B. Gustavsen, "Improving the pole relocating properties of vector fitting," *IEEE Transactions on Power Delivery,* vol. 21, no. 3, pp. 1587-1592, July 2006.

[6] D. Deschrijver, M. Mrozowski, T. Dhaene and D. De Zutter, "Macromodeling of Multiport Systems Using a Fast Implementation of the Vector Fitting Method," *IEEE Microwave and Wireless Components Letters,* vol. 18, no. 6, pp. 383-385, June 2008.

[7] H. Hotelling, "Analysis of a complex of statistical variables into principal components," *Journal of Educational Psychology,* vol. 24, no. 6, pp. 417-441, 1933.

[8] S. Wold, K. Esbensen and P. Geladi, "Proceedings of the Multivariate Statistical Workshop for Geologists and Geochemists Principal component analysis," *Chemometrics and Intelligent Laboratory Systems,* vol. 2, no. 1, pp. 37-52, 1987.

[9] H. Abdi and L. J. Williams, "Principal component analysis," *Wiley Interdisciplinary Reviews: Computational Statistics,* vol. 2, no. 4, pp. 433-459, 2010.

[10] M. Rosenblatt, "Remarks on Some Nonparametric Estimates of a Density Function," *Ann. Math. Statist.,* vol. 27, no. 3, pp. 832-837, Nov. 1956.

[11] E. Parzen, "On Estimation of a Probability Density Function and Mode," *Ann. Math. Statist.,* vol. 33, no. 3, pp. 1065-1076, Sept. 1962.

[12] M. Kristan, A. Leonardis and D. Skočaj, "Multivariate online kernel density estimation with Gaussian kernels," *Pattern Recognition,* vol. 44, no. 10-11, pp. 2630-2642, 2011.